Research Article | Vol. 27, No. 24 / 25 November 2019 / Optics Express 35600
Optics EXPRESS

Ultra-small photonic crystal (PhC)-based test tool for gas permeability of polymers

QIFENG QIAO,[1,2,3] CHENYU PENG,[1] JI XIA,[1] CHENGKUO LEE,[2,3,4] AND GUANGYA ZHOU[1,3,5]

[1]Department of Mechanical Engineering, National University of Singapore, 117579, Singapore
[2]Department of Electrical and Computer Engineering, National University of Singapore, 117583, Singapore
[3]Center for Intelligent Sensors and MEMS (CISM), National University of Singapore, 117608, Singapore
[4]elelc@nus.edu.sg
[5]mpezgy@nus.edu.sg

Abstract: We present an ultra-small photonic crystal-based test tool for gas permeability of polymers. It features a fully-etched photonic crystal (PhC) structure occupying an area of 20 μm × 800 μm on silicon-on-insulator wafer. The light-matter interaction in the PhC cavity with deformed Polydimethylsiloxane (PDMS) under pressure difference was investigated with finite element method and finite-difference time-domain method numerically. Next, three PDMS membranes of different mixing ratios were utilized for the characterization of gas permeation flux. The feasibility and effectiveness of the proposed working mechanism are verified through clearly distinguishing the gas permeability of these three testing samples. Compared with conventional test tools, this proposed test tool has fast response while it consumes less testing gas volume in a testing system with reduced footprint. Potentially, it can be integrated into lab-on-a-chip devices to measure gas permeation in nano scale.

© 2019 Optical Society of America under the terms of the OSA Open Access Publishing Agreement

1. Introduction

Optical sensor is an important type of sensing platforms in modern life. It is fast becoming a key instrument in industry, military and society. With the advance of micro fabrication technologies, the optical sensors can be designed in greatly compact size. The micro-scale optical sensors, which are realized through the on-chip optical microcavities [1], have advantages such as the capability of remote sensing, immunity to electromagnetic interference, small footprint and fast response. Among the optical microcavities, photonic crystal (PhC) cavity is one of the promising candidates for sensing applications because of its high ratio of quality (Q) factor to mode volume, ultra-compact size, good integration compatibility, and mature fabrication. A number of researchers have reported the PhC-based sensors for various applications in the past decade [2–12]. As the optical field interacts with the target analyte, the change of resonance wavelength and linewidth of the optical microcavity caused by the presence of analyte can be an indicator to evaluate the target sensing signal.

To further enhance the performance of PhC-based sensors, PhC nanobeam cavity is an auspicious choice. Due to the small physical footprint and mechanical design flexibility, sensors based on PhC nanobeam cavity can be well optimized to enhance the light-matter interaction [13]. With the utilization of suspended doubly coupled nanobeam cavities, optomechanical displacement sensors of outstanding performance have been demonstrated [14,15]. Besides, temperature sensors based on the thermal-optic effect have been reported [16,17]. In addition, efforts have been made on the sensing applications based on refractive index perturbation. Various kinds of refractive index sensing applications have been demonstrated, including nanoparticle sensor [18–21], bio-chemical fluidic sensor [22–25], and gas sensor [26]. Most studies on the PhC nanobeam cavity based sensor have only focused on liquid and gas sensing. However, the light-matter interaction in optical microcavity with polymer has barely been investigated.

#373916 https://doi.org/10.1364/OE.27.035600
Journal © 2019 Received 30 Jul 2019; revised 22 Oct 2019; accepted 23 Oct 2019; published 20 Nov 2019

Optics EXPRESS

There are two common methods for the determination of polymer gas permeability [27], namely differential pressure method and equal pressure method. For the first method, the sample membrane divides the permeation cavity into two independent parts with pressure difference. The testing gas permeates from the high pressure cavity to the low pressure cavity through the sample membrane. Accurate pressure sensing systems are required for both parts in the cavity. With measured pressure changes and permeation time, gas permeability of the sample membrane can be calculated with standard formulas, such as ISO 2556, ASTM D1413, etc. For the second method, the sample membrane divides the permeation cavity into two independent parts with same total pressure, but there is a partial pressure difference between the testing gas part and carrier gas part. Thus, the testing gas permeates to the carrier gas part. Then, it is sent to a chemical sensor by the carrier gas. Besides necessary pressure sensors used in the system, chemical sensors are required for the detection of testing gas in the carrier gas part. Calculation formulas for the gas permeability are offered in standards, such as ASTM D3985, ISO 10105-2, etc. Nowadays, both of the testing methods are universal and reliable to determine the gas permeability. However, most of the testing systems are bulky, which are made up of huge cavities, pipes and gauges. Thus, the testing process consumes considerable time and gas volume. Besides, several mechanical and chemical sensors are demanded for the measurements.

In this paper, the light-matter interaction in PhC nanobeam cavity with deformed polymer is investigated. Moreover, a 20 μm × 800 μm PhC-based test tool for polymer gas permeability is proposed. Compared with conventional test tools, this ultra-small test tool can greatly save the testing time and gas volume. The numerical investigations on the light-matter interaction in PhC cavity with deformed membrane are presented. Polydimethylsiloxane (PDMS) membranes of different mixing ratio offering gas permeability variations [28] are adopted to validate the proposed test tool experimentally.

2. Working principle

The schematic of proposed test tool is illustrated in Fig. 1(a). The whole device is formed on the silicon-on-insulator (SOI) wafer. The fully-etched PhC-based grating couplers [29] are connected with the center PhC nanobeam cavity through tapered waveguides. The PDMS membrane is used as the testing sample in this paper. It is transferred onto the silicon device layer for testing. As the testing membrane is much larger than the functional device area, air inside the etched trenches and holes are tightly confined in the cavity between testing sample and SOI, thereby forming a sealed cavity. The light can still propagate in the silicon waveguide because the refractive index of PMDS is lower than silicon [30].

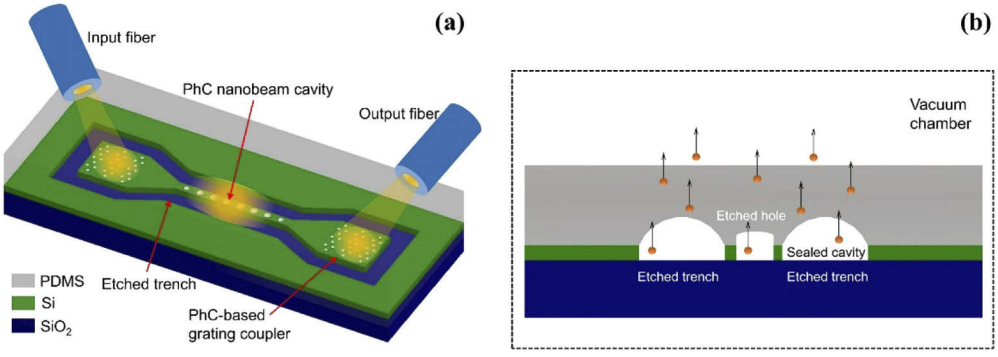

Fig. 1. (a) Schematic of the proposed test tool; (b) The gas permeation and membrane deformation caused by pressure difference.

Optics EXPRESS

The free-space fibers are aligned above the PDMS membrane so that light can be coupled in and out of the on-chip device through grating couplers. As shown in Fig. 1(b), the proposed test tool is placed in a vacuum chamber with a pumping station for the test. The testing membrane separates the sealed cavity from surrounding environment. Before the pumping starts, the resonance shift ($\Delta\lambda$) of PhC nanobeam cavity is zero in the ambient pressure environment (p_0). Once the pumping starts, the testing gas starts to permeate from the sealed cavity to the vacuum chamber due to the pressure difference. Meanwhile, the pressure difference between two sides of the testing membrane causes membrane deformation above the etched holes and trenches as shown in Fig. 1(b), thereby inducing the variations of $\Delta\lambda$. It is assumed that the chamber pressure could decrease rapidly to a low and stable pressure (p_1). As the testing membrane is gas permeable, the sealed cavity pressure gradually drops down to vacuum chamber pressure. After pumping time t_p, the dropping of pressure difference takes the PDMS back to flat shape, thereby bringing $\Delta\lambda$ back to zero. Therefore, the time measurements of PhC cavity resonance shift can be used to evaluate the pressure difference, which also denote the gas permeation situation.

Considering the testing membrane is flat under equal pressure situation, the volume of testing gas in sealed cavity at t_p can be assumed as the same with volume V_0 before pumping. The variation of temperature T_0 during the test is assumed to be negligible. From the ideal gas law, the initial moles amount of testing gas in sealed cavity can be given by $n_0 = (p_0 V_0 / RT_0)$ where R is the ideal gas constant, while the moles amount of testing gas at t_p can be given by $n_1 = (p_1 V_0 / RT_0)$. Therefore, the testing membrane permeation flux is given by

$$J = \frac{n_0 - n_1}{A t_p} = \frac{V_0(p_0 - p_1)}{ART_0 t_p}, \tag{1}$$

where p_0 is the ambient pressure, p_1 is the vacuum pressure, t_p is the permeation time for $\Delta\lambda$ to return zero and A is the effective permeation area on the membrane. A is assumed to be the etched area on the Si layer. In this way, the membrane gas permeation flux is defined as the moles amount of gas flowing through the membrane per unit area per unit time.

The working principle of the proposed test tool is illustrated as above for the permeability test of air. It is noteworthy that the proposed test tool can also be applied to other different testing gas. For a specific testing gas, it is required to be filled in the sealed cavity before the permeability test. Firstly, the vacuum chamber is evacuated and maintained vacuum for the net emission of air in both the chamber and sealed cavity. Then, the specific testing gas is pumped into the chamber and maintained at a pressure p_0. As the testing membrane is gas permeable, the sealed cavity will be filled with the specific testing gas of pressure p_0. Next, we can start the permeability test for the specific gas with use of the abovementioned operation.

3. Device design and numerical analysis

To investigate the light-matter interaction in PhC nanobeam cavity with testing PDMS membrane under pressure difference, numerical analyses were carried out. Based on the combination of finite element method (FEM) and finite-difference time-domain (FDTD) simulation results, the optical resonance shifts of the test tool induced by different surrounding pressure were given. First, the resonance wavelength (λ_{res}), Q factor and effective mode volume (V_{eff}) of the PhC nanobeam cavity were calculated. V_{eff} is the effective mode volume normalized by $(\lambda_{res}/n)^3$, where n = 3.46 for silicon. The PhC nanobeam cavity was designed with the principles proposed by Quan et al. [31,32]. Specifically, the whole device was formed on a SOI wafer with 260 nm thick Si device layer and 1 μm thick buried oxide layer. The nanobeam waveguide was 700 nm wide, and 80 air holes were etched on it. These holes were placed in a periodicity of 300 nm. Their radii were quadratically tapered from 100 nm (center) to 60 nm (side) after 39 periodic units. The 2 μm wide trenches were fully etched along both sides of the waveguide. This design

Optics EXPRESS

has the advantages of high Q factor and low mode volume, which are favorable for the sensing applications. The simulation results are summarized in Table 1.

Table 1. 3D FDTD simulation results of the PhC nanobeam cavity on 1 μm buried oxide layer.

TE mode	1st order	2nd order	3rd order
Resonance wavelength (nm)	1532.670	1550.830	1563.920
Q factor	6×10^6	3.5×10^6	5×10^5
Effective mode volume	1.06	1.7	1.86

The FEM simulations of PDMS deformation were carried out with COMSOL Multiphysics. A 100 μm thick PDMS membrane was placed on the Si device layer. Considering the PDMS membrane was tightly bonded with Si layer, the pressure applied area was defined on the PDMS membrane above 2 μm wide etched trenches and 80 etched holes. As shown in Fig. 2(a), 9990 Pa was applied in Y-axis on the selected area.

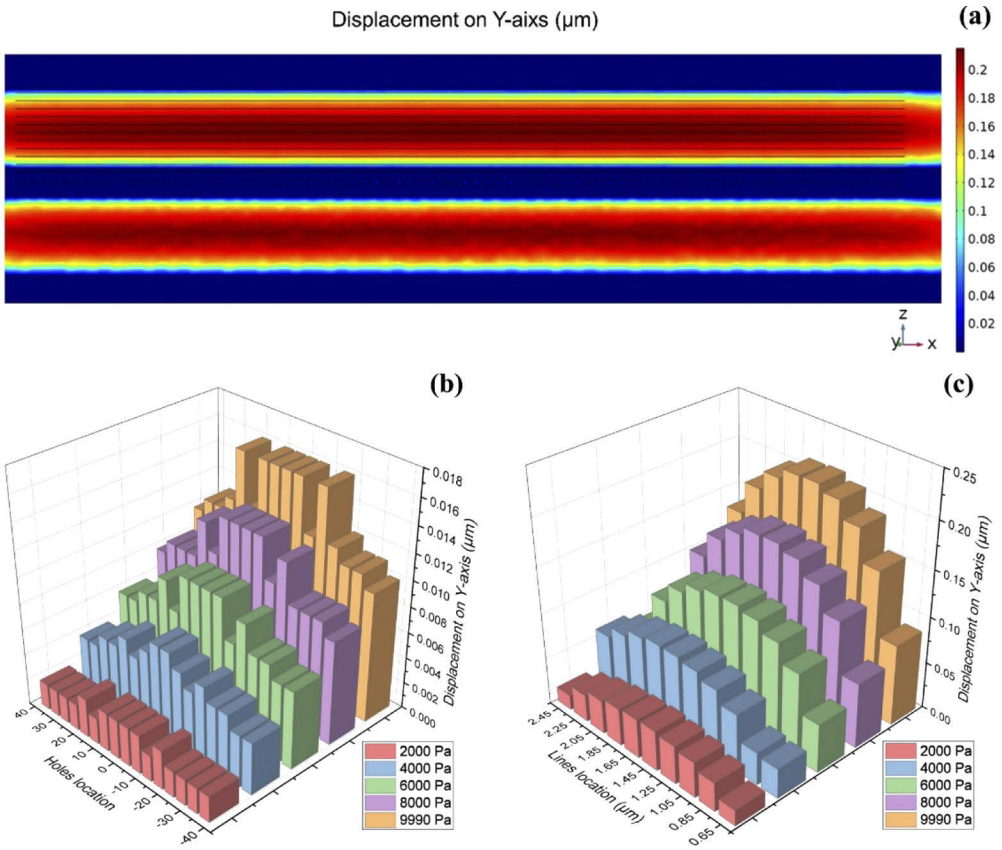

Fig. 2. FEM simulation results and derived values. (a) Deformation of PDMS membrane under 9990 Pa pressure applied; (b) Derived values of average displacement above etched holes under different applied pressure. The holes locations are numbered as 0 in the center and ± 40 in the side; (c) Derived values of average displacement above etched trenches under different applied pressure. The lines locations are denoted with the distance from the center line of nanobeam.

Due to the small area of the etched holes, only little deformation of PDMS was caused above them. There were eighty points added on every center of the etched holes. The displacement

Optics EXPRESS

values were derived from these points, and every five points were averaged to simplify the derived model. The obtained displacement values above etched holes are plotted in Fig. 2(b). Similarly, the displacement values above etched trenches were derived from the averages on the lines. There were ten lines added in equal interval on the etched trenches. The derived displacement values above etched trenches are plotted in Fig. 2(c).

Based on the derived displacement values, the deformed geometry under pressure difference was built in Lumerical FDTD Solutions. As the sectional view in Fig. 3(a) shows, the deformed model was simplified with the derived values. The third order transverse-electric(TE_3) mode was selected due to its high transmission. 3D FDTD simulations were carried out to characterize the resonance shift of TE_3 as a function of pressure difference between two sides of the PDMS membrane. The refractive index of PDMS was set to be 1.4. Figure 3(b) shows the FDTD simulation results.

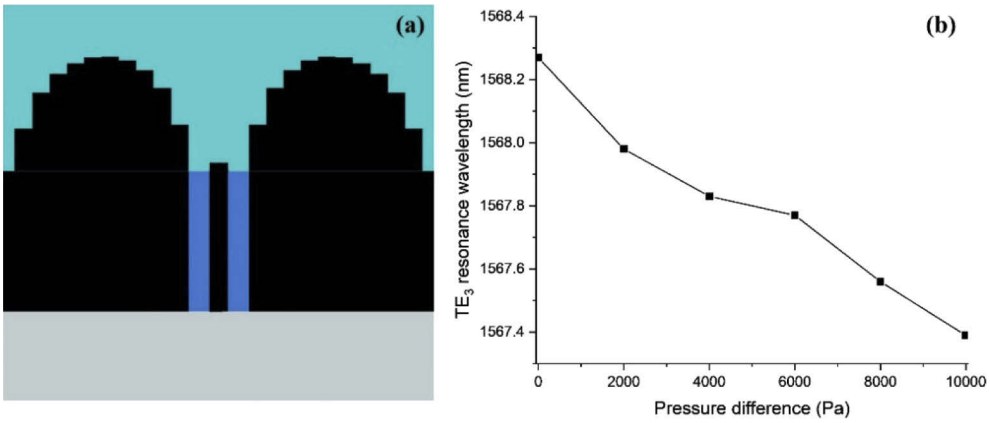

Fig. 3. FDTD simulation results. (a) Sectional view of geometric model. The green, blue, grey and black part denote PDMS, Si, SiO_2 and air respectively. (b) The relationship between TE_3 resonance wavelength and pressure difference.

From the numerical analysis, it can be found that the light-matter interaction is strong enough to induce resonance shift of the optical microcavity. The TE_3 resonance shift with pressure difference is characterized as 8.8 nm/MPa, which is promising for further experimental validation. These simulation results suggest that the expansion of sealed cavity caused by pressure difference can induce blueshift of the resonance wavelength.

4. Experimental measurements and discussion

First, the PhC nanobeam cavity was tested before the gas permeability testing. The device was fabricated on a SOI wafer. Electron beam lithography (EBL) was employed to pattern the whole structure on the photoresist ZEP 520A. After removal of the exposed photoresist using Amyl acetate developer, deep reactive ion etching (DRIE) was carried out to fully etch the exposed Si device layer. Figure 4(a) shows top-view SEM images of the device. The experimental setup basically consisted of a tunable laser source (TLS, ANDO AQ4321D), an optical spectrum analyzer (OSA, ANDO AQ6317C) and a vacuum chamber. The schematic is shown in Fig. 4(a). The light was launched from the TLS (1.52 μm~1.62 μm) to the OSA through the proposed test tool. With the coupling between the fibers and grating couplers, light was coupled in and out of the test tool. The optical circuit was maintained during the pumping with use of the fiber feedthroughs on vacuum chamber. After the precise alignment under microscope, the vacuum chamber could be closed to create a totally sealed condition. Figure 4(b) shows the measured transmission spectrum. As the results of Lorentz fitting, the resonance of TE_2 was located at

Optics EXPRESS

wavelength 1563.773 nm with a Q factor of 11000, while the resonance of TE_3 was located at wavelength 1573.261 nm with a Q factor of 4000. The deviations of resonance wavelength and degradation of Q factor from simulation results were caused by the fabrication imperfections.

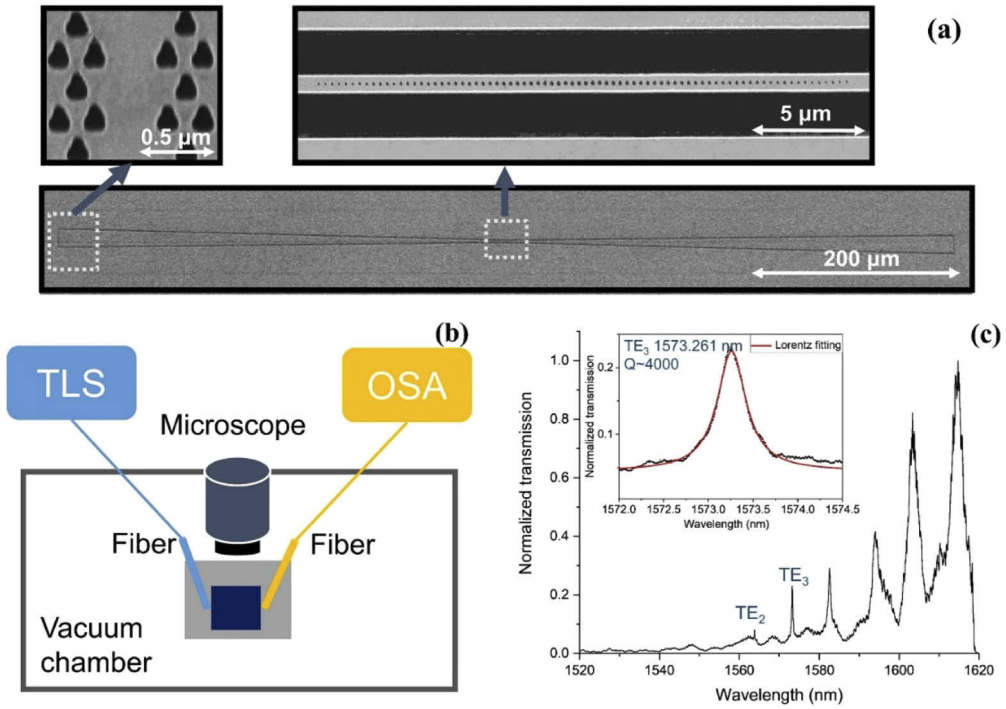

Fig. 4. (a) SEM images of the proposed test tool; (b) Schematic of experimental setup; (c) Transmission spectrum of the PhC nanobeam cavity (1.52μm~1.62μm) and Lorentz fitting of TE_3 in the inset.

Next, three PDMS membranes with different mixing ratio were prepared for the gas permeability test. The polymer base and curing agent (Sylgard 184, Dow Corning) were mixed in different weight ratios (5:1, 10:1, 20:1). The photoresist PMMA 495K A5 was used as a sacrificial layer on the SOI wafer first. On the top of it, PDMS membrane was prepared with spin coating and post baking. Three 100 μm thick membranes of different mixing ratios were formed with identical settings of spin coating. Finally, the PDMS membranes were released from the sacrificial layer with acetone rinsing. Gas permeation flux variations were provided with these three PDMS membrane with different mixing ratio [28]. In the following content, the three testing samples were denoted as PDMS 5:1, PDMS 10:1and PDMS 20:1 according to their mixing ratio. Then, the PDMS membrane was transferred onto the proposed test tool for experimental characterization. The resonance mode TE_3 was chosen for the measurements because of its high transmission. The pressure of vacuum chamber could be read out from the commercial pumping station (Pfeiffer Vacuum HiCube Pumping Station). The vacuum chamber pressure decayed from 10^5 Pa to 10^2 Pa after 20 minutes pumping.

Three PDMS samples were tested in turn. PDMS 5:1 was tested first, which had the lowest air permeability among these three samples. The transmission spectrums of TE_3 resonance at three time points are plotted in Fig. 5(a). It could be found that blueshift of the resonance wavelength was caused after the pumping started. The time measurements of TE_3 resonance wavelength for PDMS 5:1 are shown in Fig. 5(b). After 40 minutes pumping, the resonance shift fell down to the lowest point as −1.2 nm. Then, it rose gradually to be stable as −0.7 nm after 120 min

Optics EXPRESS

pumping. The blueshift of resonance at the start of pumping was in consistent with what has been found in numerical analysis. It took some time for $\Delta\lambda$ to fall to the lowest value because the pumping rate in the experiment was not so large as supposed. It took 20 minutes for the vacuum chamber pressure to reach 10^2 Pa.

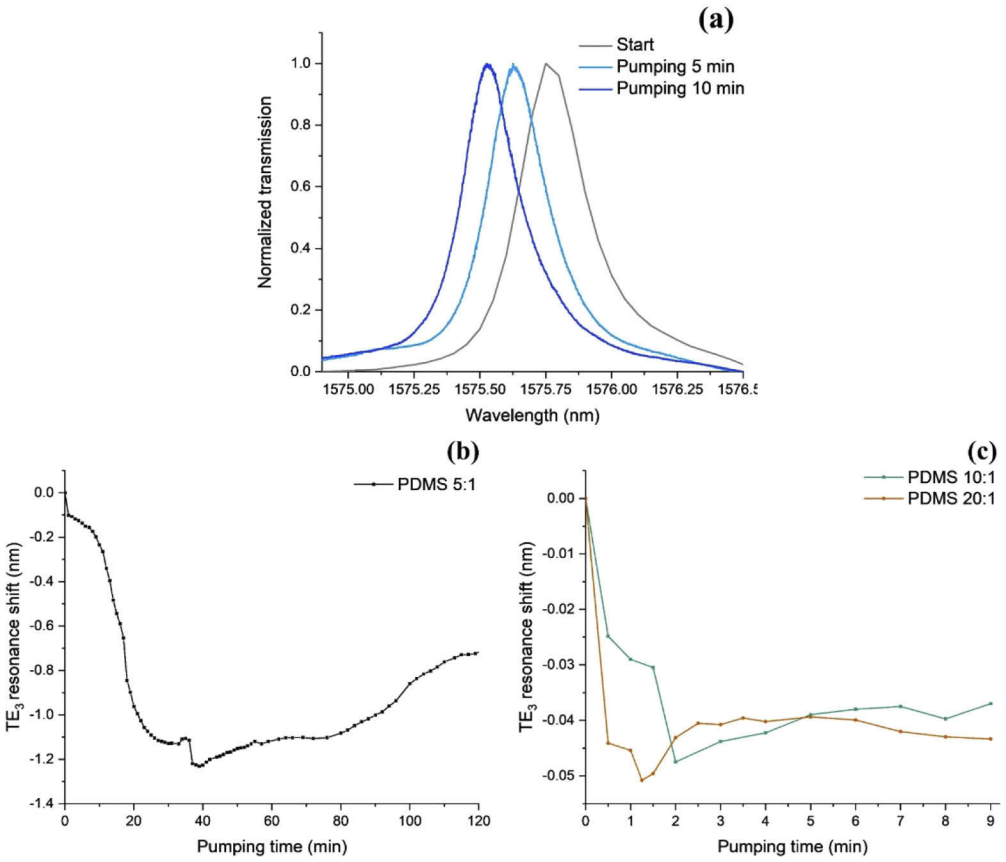

Fig. 5. Experimental results. (a) Measurements of PDMS 5:1 at three time points; (b) Time measurements of resonance shift for PDMS 5:1; (c) Time measurements of resonance shift for PDMS 10:1 and PDMS 20:1.

From Fig. 5(b) and Fig. 5(c), it can be seen that $\Delta\lambda$ turns to a negative value at last in these three experiments. However, it should have returned zero as predicted. The PDMS membrane was tightly bonded on Si layer before pumping, while it could be slightly peeled off from the Si layer due to the gas flow during the test. At the end of test, though the elimination of pressure difference took the PDMS membrane back to a flat shape, the minor air gap on the edges of waveguides and holes caused by gas flow could bring $\Delta\lambda$ to a stable negative value. Hence, the definition of t_p is modified to be the pumping time required for the resonance shift to return stable, and the definition of p_1 is modified to be the vacuum chamber pressure at t_p.

In this way, t_p of PDMS 5:1, PDMS 10:1 and PDMS 20:1 were measured as 120 min, 7 min and 3.5 min respectively. With the pressure measurements from the pumping station, p_1 of PDMS 5:1, PDMS 10:1 and PDMS 20:1 were recorded as 540 Pa, 220 Pa and 34 Pa respectively. As introduced above, the testing sample permeation flux was given by $J = V_0(p_0 - p_1)/(ART_0t_p)$. Thus, the relative gas permeation flux among PDMS 5:1, PDMS 10:1 and PDMS 20:1 were

Optics EXPRESS

given as 1:17:34. In line with previous study [28], the permeation flux of PDMS samples were enhanced by increasing the mixing ratio.

Due to the highly permeable testing sample used in the latter two tests, the sealed cavity pressure decreased quickly once the pumping started. Therefore, the lowest point that the resonance shift reached in these two tests was −0.05 nm, which was not so far as −1.2 nm in the first test for PDMS 5:1. This suggested that the PDMS deformation in the latter two tests was smaller than the one in the first test.

From the experimental results, the working mechanism of this proposed test tool is validated. With the time measurements of resonance shift and vacuum chamber pressure, the testing membrane gas permeation flux can be given in the unit mol·μm^{-2}/min. In the common test methods for membrane gas permeability, Barrer is used as the unit, which measures the flow rate in unit area of a membrane with a thickness by a given pressure. Due to the limitations of our experimental conditions, it is hard to maintain a large and constant pressure difference throughout the experiment. Thus, we utilize a time average of gas permeation to define the gas permeation flux. With the test of gas permeation flux, we can compare the gas permeability of the samples. As results, a sharp contrast of gas permeability among three testing samples are obtained. For the calibration of permeability coefficient, the testing system and mathematical model need to be further developed.

5. Conclusion

In this paper, we demonstrate a micro-scale PhC-based test tool for gas permeability of polymers numerically and experimentally. Based on FEM and FDTD simulations, the resonance shifts of PhC cavity induced by PDMS deformation under pressure difference are given as 8.8 nm/MPa. The gas permeability of three PDMS samples could be clearly distinguished experimentally through the time measurements of resonance shift and vacuum chamber pressure. As results, the relative gas permeation flux among PDMS 5:1, PDMS 10:1 and PDMS 20:1 were given as 1:17:34. In this proposed test tool, the micro device in Si layer works as the testing gas cavity and optical sensor simultaneously. Such a micro-scale test tool can greatly reduce the size of gas permeability testing system. Compared with the conventional test tools, it can considerably save the testing gas volume and testing time due to the micro volume of this test tool. Moreover, the fully-etched PhC structure can be easily fabricated. Through engineering the device layer material, cavity and trench design, the proposed working mechanism can be applied to gas permeability test for many kinds of polymers.

Funding

National Research Foundation Singapore (R-263-000-C24-281, R-263-000-C64-281); Agency for Science, Technology and Research (R-263-000-C91-305).

References

1. K. J. Vahala, "Optical microcavities," Nature **424**(6950), 839–846 (2003).
2. E. Chow, A. Grot, L. Mirkarimi, M. Sigalas, and G. Girolami, "Ultracompact biochemical sensor built with two-dimensional photonic crystal microcavity," Opt. Lett. **29**(10), 1093–1095 (2004).
3. A. Di Falco, L. O'faolain, and T. Krauss, "Chemical sensing in slotted photonic crystal heterostructure cavities," Appl. Phys. Lett. **94**(6), 063503 (2009).
4. S. Zlatanovic, L. W. Mirkarimi, M. M. Sigalas, M. A. Bynum, E. Chow, K. M. Robotti, G. W. Burr, S. Esener, and A. Grot, "Photonic crystal microcavity sensor for ultracompact monitoring of reaction kinetics and protein concentration," Sens. Actuators, B **141**(1), 13–19 (2009).
5. W. C. Lai, S. Chakravarty, Y. Zou, and R. T. Chen, "Silicon nano-membrane based photonic crystal microcavities for high sensitivity bio-sensing," Opt. Lett. **37**(7), 1208–1210 (2012).
6. C. Caër, S. F. Serna-Otálvaro, W. Zhang, X. Le Roux, and E. Cassan, "Liquid sensor based on high-Q slot photonic crystal cavity in silicon-on-insulator configuration," Opt. Lett. **39**(20), 5792–5794 (2014).

Optics EXPRESS

7. S. Chakravarty, A. Hosseini, X. Xu, L. Zhu, Y. Zou, and R. T. Chen, "Analysis of ultra-high sensitivity configuration in chip-integrated photonic crystal microcavity bio-sensors," Appl. Phys. Lett. **104**(19), 191109 (2014).
8. J. Wei, F. Sun, B. Dong, Y. Ma, Y. Chang, H. Tian, and C. Lee, "Deterministic aperiodic photonic crystal nanobeam supporting adjustable multiple mode-matched resonances," Opt. Lett. **43**(21), 5407–5410 (2018).
9. Y. Ma, B. Dong, B. Li, K.-W. Ang, and C. Lee, "Dispersion engineering and thermo-optic tuning in mid-infrared photonic crystal slow light waveguides on silicon-on-insulator," Opt. Lett. **43**(22), 5504–5507 (2018).
10. B. Dong, T. Hu, X. Luo, Y. Chang, X. Guo, H. Wang, D.-L. Kwong, G.-Q. Lo, and C. Lee, "Wavelength-Flattened Directional Coupler Based Mid-Infrared Chemical Sensor Using Bragg Wavelength in Subwavelength Grating Structure," Nanomaterials **8**(11), 893 (2018).
11. Y. Chang, D. Hasan, B. Dong, J. Wei, Y. Ma, G. Zhou, K. W. Ang, and C. Lee, "All-dielectric surface-enhanced infrared absorption-based gas sensor using guided resonance," ACS Appl. Mater. Interfaces **10**(44), 38272–38279 (2018).
12. Z. Ren, Y. Chang, Y. Ma, K. Shih, B. Dong, and C. Lee, "Leveraging of MEMS Technologies for Optical Metamaterials Applications," *Adv. Opt. Mater.*, 1900653 (2019).
13. Q. Qiao, J. Xia, C. Lee, and G. Zhou, "Applications of photonic crystal nanobeam cavities for sensing," Micromachines **9**(11), 541 (2018).
14. A. G. Krause, M. Winger, T. D. Blasius, Q. Lin, and O. Painter, "A high-resolution microchip optomechanical accelerometer," Nat. Photonics **6**(11), 768–772 (2012).
15. H. Du, G. Zhou, Y. Zhao, G. Chen, and F. S. Chau, "Magnetic field sensor based on coupled photonic crystal nanobeam cavities," Appl. Phys. Lett. **110**(6), 061110 (2017).
16. Y. Zhang, P. Liu, S. Zhang, W. Liu, J. Chen, and Y. Shi, "High sensitivity temperature sensor based on cascaded silicon photonic crystal nanobeam cavities," Opt. Express **24**(20), 23037–23043 (2016).
17. P. Liu and Y. Shi, "Simultaneous measurement of refractive index and temperature using cascaded side-coupled photonic crystal nanobeam cavities," Opt. Express **25**(23), 28398–28406 (2017).
18. F. Liang and Q. Quan, "Detecting Single Gold Nanoparticles (1.8 nm) with Ultrahigh-Q Air-Mode Photonic Crystal Nanobeam Cavities," ACS Photonics **2**(12), 1692–1697 (2015).
19. B. Schmidt, V. Almeida, C. Manolatou, S. Preble, and M. Lipson, "Nanocavity in a silicon waveguide for ultrasensitive nanoparticle detection," Appl. Phys. Lett. **85**(21), 4854–4856 (2004).
20. S. Lin, J. Hu, L. Kimerling, and K. Crozier, "Design of nanoslotted photonic crystal waveguide cavities for single nanoparticle trapping and detection," Opt. Lett. **34**(21), 3451–3453 (2009).
21. S. Lin and K. B. Crozier, "Trapping-assisted sensing of particles and proteins using on-chip optical microcavities," ACS Nano **7**(2), 1725–1730 (2013).
22. X. Zhang, G. Zhou, P. Shi, H. Du, T. Lin, J. Teng, and F. S. Chau, "On-chip integrated optofluidic complex refractive index sensing using silicon photonic crystal nanobeam cavities," Opt. Lett. **41**(6), 1197–1200 (2016).
23. S. Mandal, X. Serey, and D. Erickson, "Nanomanipulation using silicon photonic crystal resonators," Nano Lett. **10**(1), 99–104 (2010).
24. Y. F. Chen, X. Serey, R. Sarkar, P. Chen, and D. Erickson, "Controlled photonic manipulation of proteins and other nanomaterials," Nano Lett. **12**(3), 1633–1637 (2012).
25. G. Shambat, S. R. Kothapalli, J. Provine, T. Sarmiento, J. Harris, S. S. Gambhir, and J. Vuckovic, "Single-cell photonic nanocavity probes," Nano Lett. **13**(11), 4999–5005 (2013).
26. Y. Chen, W. S. Fegadolli, W. M. Jones, A. Scherer, and M. Li, "Ultrasensitive gas-phase chemical sensing based on functionalized photonic crystal nanobeam cavities," ACS Nano **8**(1), 522–527 (2014).
27. D. Pye, H. Hoehn, and M. Panar, "Measurement of gas permeability of polymers. I. Permeabilities in constant volume/variable pressure apparatus," J. Appl. Polym. Sci. **20**(7), 1921–1931 (1976).
28. A. Lamberti, S. Marasso, and M. Cocuzza, "PDMS membranes with tunable gas permeability for microfluidic applications," RSC Adv. **4**(106), 61415–61419 (2014).
29. L. Liu, M. Pu, K. Yvind, and J. M. Hvam, "High-efficiency, large-bandwidth silicon-on-insulator grating coupler based on a fully-etched photonic crystal structure," Appl. Phys. Lett. **96**(5), 051126 (2010).
30. J. E. Mark, Polymer data handbook (Oxford University, 2009).
31. Q. Quan, P. B. Deotare, and M. Loncar, "Photonic crystal nanobeam cavity strongly coupled to the feeding waveguide," Appl. Phys. Lett. **96**(20), 203102 (2010).
32. Q. Quan and M. Loncar, "Deterministic design of wavelength scale, ultra-high Q photonic crystal nanobeam cavities," Opt. Express **19**(19), 18529–18542 (2011).

58.182.221.88 (to 2019-12-04 09:48:58)